





REGULAR PAPER

Research on lateral dynamics safety margins of carrier-based aircraft arresting

Z. Zhang^{1,2} , Y. Peng^{1,2}, T. Liang^{1,2}, X. Wei^{1,2}  and Y. Wang^{1,2}

¹State Key Laboratory of Mechanics and Control of Mechanical Structures, Nanjing University of Aeronautics and Astronautics, Nanjing, Jiangsu, China and ²Key Laboratory of Fundamental Science for National Defense-Advanced Design Technology of Flight Vehicle, Nanjing University of Aeronautics and Astronautics, Nanjing, Jiangsu, China
E-mail: wei_xiaohui@nuaa.edu.cn

Received: 22 October 2021; **Revised:** 28 December 2021; **Accepted:** 5 January 2022

Keywords: Carrier-based aircraft; Arresting; Dynamics; Safety boundary; Reachability

Abstract

For the safety problems caused by the limited landing space of the deck during the arresting process of the carrier-based aircraft, a dynamic model of the carrier-based aircraft's landing and arresting is built. Based on the batch simulation method, the lateral dynamics safety envelope of the aircraft during the arresting was defined, and the dynamic response of the key points in the envelope during the arresting process was investigated. Subsequently, the influence of engine thrust and aircraft quality on the arresting safety envelope was studied based on reasonable safety evaluation indicators, and the safety status envelope of the deck arresting was given. Then, the particular Hamilton-Jacobi partial differential equation is used to obtain the lateral dynamics safety envelope of the carrier-based aircraft in the process of landing and arresting by backward inversion. Results indicate that engine thrust and landing quality have little effect on the yaw angle in the arresting safety boundary during the arresting. Additionally, with the engine thrust and landing quality increase, the maximum safe off-center distance gradually decreases, and the safety boundary decreases accordingly. During the phase of landing glide, the engine thrust and quality have little effect on the maximum safe eccentric distance. When the engine thrust is increased by 40%, the maximum safe yaw angle is reduced from 0.3°, and the safety boundary is reduced by 4.2%. When the aircraft quality increases by 40%, the maximum safe yaw angle is reduced by 0.4°, and the safety boundary is reduced by 2.8%. The findings of this paper can provide framework for the research on the aircraft-to-carrier dynamic matching characteristics of the carrier-based system, and is of great significance to the research on improving the safety of the carrier-based aircraft landing arresting.

Nomenclature

b	the wingspan
B_a	wingspan of the aircraft
B_{deck}	the width of the landing runway
B_r	distance between wingtip and boundary
c	the mean aerodynamic chord
C	permissible state set
C_D	drag coefficient
C_L	lift coefficient
C_Y	side coefficient
C_r	the side force coefficient of the rudder
C_{δ_r}	the force generated by the rudder
d	the length of landing zone
D	half of the distance between two pulleys
D_y	off-center distance

F_{arrest}	the arresting force of the aircraft
F_C	side force
F_D	drag force
F_x	resultant force along $O_b x_b$
F_y	resultant force along $O_b y_b$
I_z	moment of inertia around $O_b z_b$
m	the quality of the aircraft
M_y	yawing moment
M_z	positive around $O_b x_b$
N	number of movable pulleys
r	angular velocity in yaw
S	displacement of aircraft
S_{deck}	the length of runway
S_f	the length of the deceleration zone
S_r	length of the revolving zone
S_{ra}	the rudder area
S_{rd}	displacement of the piston
S_{rL}	the displacement of the left piston
S_{rR}	the displacement of the right piston
S_S	the length of the reserve zone
S_w	the wing area
T_L	the left force of the arresting cable
T_R	the right force of the arresting cable
u	the longitudinal velocity
u_a	aerodynamic velocity along $O_b x_b$
U	the permissible input
v	the lateral velocity
v_a	aerodynamic velocity along $O_b y_b$
v_h	landing speed
V_a	aerodynamic velocity vector
w_a	aerodynamic velocity along $O_b z_b$
$Y_{\delta r}$	the corresponding moment
α	angle of attack
β	sideslip angle
φ	yaw angle
ρ_a	the air density

1.0 Introduction

The ability of carrier-based aircraft to safely complete the arresting process is the key to maintaining the combat effectiveness of the aircraft carrier system. For aircraft that have a relatively high speed when landing, and the landing space provided by the deck is much smaller than the runway of the roadbed airport, it brings a very great danger to the arresting of the carrier-based aircraft [1]. The arresting of the carrier-based aircraft can be roughly divided into two stages: the flight stage before the aircraft touches down the carrier and the arresting sliding stage after the aircraft touches down the carrier [2]. When carrier landing glide, the aircraft should fly along the ideal gliding trajectory angle [3–5], ensuring that the yaw angle of the aircraft and the off-centre distance are zero during arresting [6]. After the aircraft touches down the carrier, the meshing point of the arresting hook and the cable is at the midpoint of the cable, and the speed direction of the aircraft is along the centre line of the runway. However, the landing process of the aircraft is extremely complicated. Due to the influence of guidance deviation or airflow disturbance, most of the aircraft have different degree of off-centre distance and yaw angle during the landing process, which will adversely affect the safe arresting of the aircraft. Since the entire landing process of the aircraft lasts very short duration, especially the arresting process after the hook-cable meshing only lasts less than 3 seconds, and once the arresting hook mesh the cable, it is difficult for the

pilot controlling the arresting process, which is extremely prone to accidents. According to the public report, the American F-14 and EA-6B collided with the aircraft parked on the deck due to the excessive off-centre distance and yaw angle at the time of arresting, caused huge losses. It can be seen that the arresting process of aircraft is the most important part in the research of carrier-based systems. How the carrier-based aircraft complete arresting task safely and reliably is of vital importance to the research of carrier-based systems.

The arresting process of carrier-based aircraft is extremely complex and highly nonlinear, and it is very challenging to analyse the lateral dynamics and safety characteristics of the entire process. Some approaches are explored to study the dynamic safety characteristics of the arresting process of aircraft. For example, the United States has carried out a large number of flight tests and published relevant test result curves on the topic of arresting. Most of the test reports only refer to the situation of centring arrest under the condition of no off-centre or yaw. With respect to yaw arrest, only a few fitting curves of measured data have been published; however, the mechanism and theoretical analyses of yaw arrest were not disclosed [11]. Lawrence [7] analysed the main factors affecting the peak load of the arresting hook during the arresting process, including the weight, the speed and the initial off-centre distance of aircraft at the time of the landing. Through the data statistics of the arresting system, the matching formula and curve of the arresting force was obtained. Hsin [8] analysed the movement of the aircraft after touches down the deck and found that under the combined action of the arresting device and the arresting cable, the taxiing distance of the aircraft will be significantly shortened, which can effectively prevent the aircraft from rushing out of the restricted area. Zhang [9] established the off-centre and yaw arresting dynamics model of the carrier-based aircraft and performed simulations, found that carrier-based aircraft will increase the arresting distance and stopping time when arresting asymmetrically, but the peak force of arresting would be reduced. Zhang [10] analysed the movement trend of aircraft when the aircraft arresting in off-centre and yaw condition. As mentioned above, the relevant research on the arresting of carrier-based aircraft focuses on the analysis of the dynamic characteristics, while a few scholars have examined the arresting safety under the influence of asymmetrical conditions of aircraft. For example, Peng [11] considered the influence of the bending wave of the arresting cable, and studied the safety of the aircraft yaw arresting. By calculating the lateral displacement of the aircraft during the arresting, the yaw angle range to ensure the aircraft will not rush out of the safe landing area is obtained. It should be pointed out that, it is certainly feasible to study the lateral dynamics safety of carrier aircraft arresting based on the arresting characteristics of aircraft, but this method is not comprehensive. The reason is that the arresting process of the aircraft includes the gliding into the carrier before it touches down and the arresting stage after the landing, the two phases are interrelated and coupled. The flight status of the aircraft entering the descent phase directly affects the status of arresting after it touches down the deck. However, the above studies have not combined the two to analyse the safety of the aircraft's arresting and rolling. To a certain extent, this limits the development of the research on the dynamics and safety characteristics of the aircraft's arresting.

Reachable set theory helps to solve the above problems [12]. The reachable set theory is a method based on the particular Hamilton–Jacobi partial reachability analysis method to solve the survival kernel of nonlinear dynamic system, which can establish the corresponding control rate while determining the safety boundary of the system [13]. So far, extensive research studies on reachability have been carried out to solve envelope protection, ensuring the states in the target set. Lygeros [14] systematically explained that the computation of the reachability, viability, and invariance can come down to the supremum minimum (SUPMIN) and infimum minimum optimal control problems. And creatively use the Hamiltonian–Jacobi partial differential equations to establish three sets of unified solution frameworks. Allen [15] designed the LQR (linear quadratic regulator) safety set protection control based on the safety set of the aircraft's longitudinal movement. Oishi [16] applied reachability theory to determine the flight envelope of a jet airplane and effectively solved the collision avoidance between two aircrafts. Wang [17] conducted a reachable set analysis based on the longitudinal dynamics model of the aircraft. Many existing literature shows that reachability method is mainly adopted in the longitudinal dynamics of aerial flight. It has not been introduced into the lateral motion of the aircraft. In addition,

most research on reachable sets fails to scientifically give the origin of the target set, and only analyses it as the target of the solution, which lacks the coherence of systematic research. It must be pointed out that, for the safety of the lateral dynamics of the carrier-based aircraft's arresting, it is difficult to ensure the relevance and systematisation of the entire process if the arresting or the landing of the aircraft is analysed and studied separately. Aiming at these problems, this paper determined the safety boundary of the landing arresting on the deck, and combined with the new perspective of reachable set analysis, the lateral dynamic safety boundary of the aircraft landing stage is reversely deduced to ensure that the initial off-centre distance and yaw angle of the aircraft meeting the index requirements before touches down the deck. The research results thoroughly explain the dynamic safety issues of the carrier-based aircraft during the landing arresting process, make up for the lack of related research, provided more targeted solutions for the safety of the carrier-based aircraft, and guide the subsequent design of the carrier-based system.

This study is organised as follows: Section 2 explain the working principle of the arresting system and establishes the arresting dynamic model. Reachability theory and the mathematical formulation are presented in section 3. Section 4 provides the lateral dynamics safety boundary of the carrier aircraft during the arresting and rolling process based on the batch simulation. And discusses the arresting characteristics of key points within the boundary, the influence of different landing parameters on the boundary of the arresting is analysed. Section 4 also proposed a reasonable safety evaluation index of the aircraft's arresting and rolling, and the influence of landing parameters on the safety of arresting is analysed. Then, according to the defined deck safety boundary, the lateral dynamic safety boundary of the carrier-based aircraft during the landing stage is defined based on reachability theory, and the influence of different parameters on the safety boundary is also analysed in section 6. Section 6 is the conclusion.

2.0 Dynamic model of the arresting process of carrier-based aircraft

In the process of landing arresting, the carrier-based aircraft approaches the carrier along a certain descent path at a particular airspeed. When the arresting hook mesh the arresting cable, the hook transmits the arresting force generated by the arresting device to the fuselage through the cable and the hook, thereby forcing the aircraft to slow down, and stop in a safe area within 3 seconds. Therefore, the decelerating characteristics of the aircraft after arresting is one of the important factors that affect its lateral motion on the deck [18], and it is also an important factor that determines the safety characteristics of arrest.

Figure 1 shows the schematic diagram of the carrier-based aircraft arresting system. It can be seen that the force state of the aircraft after arresting is more complicated. the arresting hook mesh the arresting cable on the deck runway, the cable bypasses the dynamic and static pulley blocks and is connected to the hydraulic arresting devices on both sides of the deck. Therefore, it is necessary to analyse the arresting force provided by the arresting device, and study the characteristics of lateral movement of carrier-based aircraft during arresting.

2.1 Calculation model of arresting force

In order to facilitate the analysis of the dynamic characteristics of the carrier-based aircraft, the force of the aircraft during the arresting process is simplified as follows [2]:

- 1) The runway is flat, and the course of the aircraft is parallel to the pavement.
- 2) The vibration after the hook-cable meshing and the influence of the bending wave of the cable are not considered during the arresting process.
- 3) The friction between the arresting hook and the arresting cable is ignored.
- 4) The corrective ability of the arresting device, and assume that the taxiing direction of the aircraft will not change with the change of arresting force.

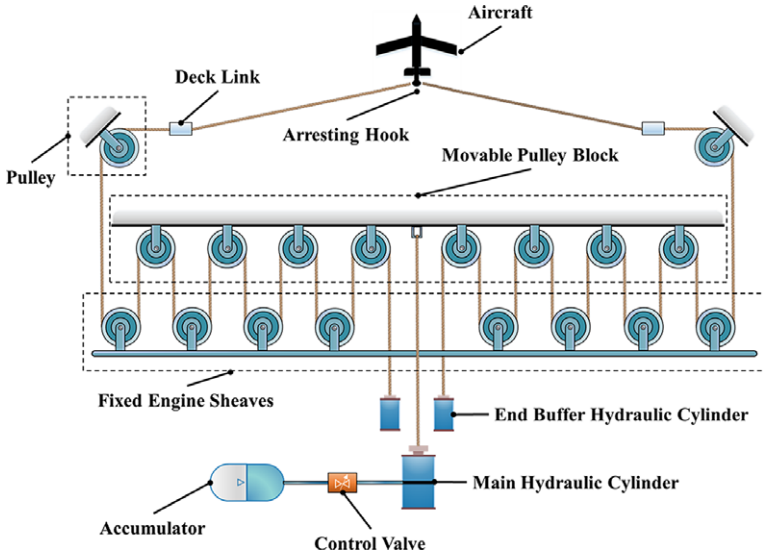


Figure 1. Schematic diagram of landing and cable hanging of carrier-based aircraft.

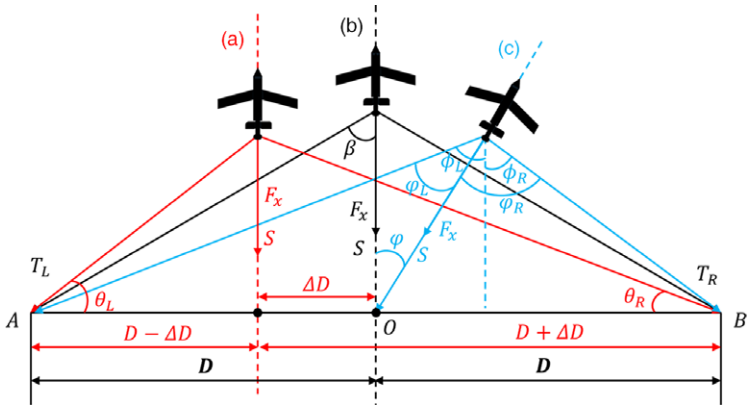


Figure 2. Schematic diagram of arresting force.

There are three situations in the arresting and rolling process of carrier-based aircraft, including (a) off-centre arresting, (b) symmetry arresting, and (c) yaw arresting. The arresting force of the aircraft under the three conditions is analysed as shown in Fig. 2

As shown in Fig. 2(a), in the case of off-centre arrest, taking left off-centre as an example, the formula for calculating the arresting force is:

$$\begin{cases} F_{arrest} = T_L \sin \theta_L + T_R \sin \theta_R \\ \sin \theta_L = \frac{S}{\sqrt{(D - \Delta D)^2 + S^2}} \\ \sin \theta_R = \frac{S}{\sqrt{(D + \Delta D)^2 + S^2}} \end{cases} \tag{1}$$

where θ_L is the angle between the left arresting cable and the connecting line of the two pulleys, θ_R is the angle between the right arresting cable and the connecting line of the two pulleys, T_L is the left

force of the arresting cable, T_R is the right force of the arresting cable, D is half of the distance between the two pulleys on the deck, ΔD is the off-centre distance, and S is the displacement of aircraft.

As shown in Fig. 2(b), in the case of centre arrest, the formula for calculating the arresting force is:

$$\begin{cases} F_{arrest} = T_L \cos \beta_h + T_R \cos \beta_h \\ \cos \beta_h = \frac{S}{\sqrt{S^2 + D^2}} \end{cases} \quad (2)$$

where F_{arrest} is the arresting force of the aircraft, T_L is the left force of the arresting cable, T_R is the right force of the arresting cable, $T_L = T_R$ when centre arresting, and β is the angle between the line of hook-pulley and the aircraft taxiing direction.

As shown in Fig. 2(c), in the case of yaw arrest, taking right yaw as an example, the formula for calculating the arresting force is:

$$\begin{cases} F_{arrest} = T_L \cos \varphi_L + T_R \cos \varphi_R \\ \varphi_L = \beta_L - \varphi, \varphi_R = \beta_R + \varphi \\ \cos \beta_L = \frac{S \cos \varphi}{\sqrt{(D + S \sin \varphi)^2 + (S \cos \varphi)^2}} \\ \cos \beta_R = \frac{S \cos \varphi}{\sqrt{(D - S \sin \varphi)^2 + (S \cos \varphi)^2}} \end{cases} \quad (3)$$

where φ is the yaw angle, φ_L is the angle between the line of hook connecting the pulley on the left deck and the midpoint of the arresting cable on the deck, and β_L is the angle between the line of hook-left pulley and the aircraft taxiing direction.

2.2 Calculation model of arresting device

To calculate the arresting force, a dynamic model of the arresting device should be established. The damping force of the arresting device is provided by the energy absorber, and the damping force output by the energy absorber is related to the movement displacement of the discharge flow control valve, the area of the oil hole on the valve, and the internal pressure of the accumulator [11]. The working principle of the energy absorber of the arresting device is shown in Fig. 3.

For a certain arresting system, the output of the force is related to the damper stroke, and the same elongation of the cable corresponds to the same cable tension [19]. The main differences in the arresting process in the three cases in Fig. 2 are: There is a difference in the length of the initial cable on the left and right of the arresting hook, which results in the different extension speeds of the cables from the left and right pulleys, and finally causes the displacement and speed of the pistons on both sides to be different. So it can be concluded:

For the case of left off-centre arrest for aircraft, the piston displacement and movement speed are:

$$\begin{cases} S_{rL} = \frac{\sqrt{S^2 + (D - \Delta D)^2} - (D - \Delta D)}{N} \\ S_{rR} = \frac{\sqrt{S^2 + (D + \Delta D)^2} - (D + \Delta D)}{N} \\ v_{rL} = \frac{S}{N\sqrt{S^2 + (D - \Delta D)^2}} v \\ v_{rR} = \frac{S}{N\sqrt{S^2 + (D + \Delta D)^2}} v \end{cases} \quad (4)$$

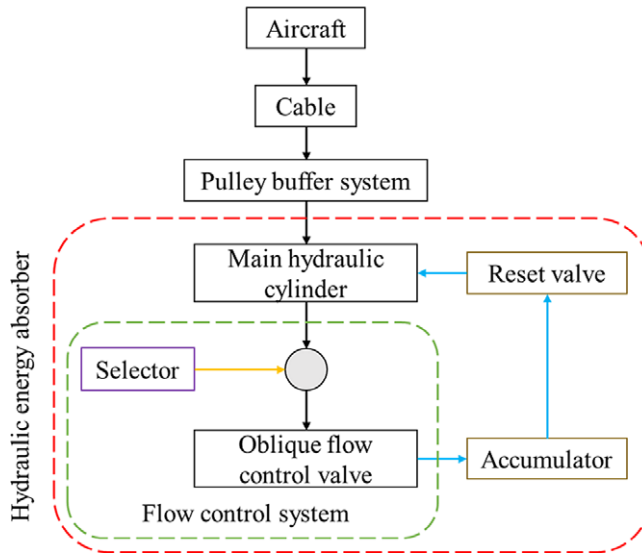


Figure 3. Principle diagram of the arresting gear energy absorber.

where S_{rL} is the displacement of the left piston, S_{rR} is the displacement of the right piston, v_{rL} is the speed of the left piston, and v_{rR} is the speed of the left piston.

For the case of symmetrical arrest, the piston displacement and movement speed are:

$$\begin{cases} S_r d = \frac{\sqrt{S^2 + D^2} - D}{N} \\ v_r = \frac{S}{N\sqrt{S^2 + D^2}} v \end{cases} \tag{5}$$

where N is the number of movable pulleys in the movable pulley group, $S_r d$ is the displacement of the piston, and v is the speed of the aircraft.

For the case of right yaw of the aircraft, the piston displacement and movement speed are:

$$\begin{cases} S_{rL} = \frac{\sqrt{(D + S \sin \varphi)^2 + (S \cos \varphi)^2} - D}{N} \\ S_{rR} = \frac{\sqrt{(D - S \sin \varphi)^2 + (S \cos \varphi)^2} - D}{N} \\ v_{rL} = \frac{v \cos \varphi_L}{N} \\ v_{rR} = \frac{v \cos \varphi_R}{N} \end{cases} \tag{6}$$

3.0 Lateral dynamics model of the aircraft entering the descent phase

In this section, the longitudinal movement of the aircraft and the movement characteristics of the deck are ignored, and three coordinates are used to build the dynamic model: ground axis system ($O_g x_g y_g$), the body axis system ($O_b x_b y_b$) and the air axis system ($O_a x_a y_a$).

The movement characteristics of the deck is ignored, and regards the deck coordinate system as the same as the ground coordinate system.

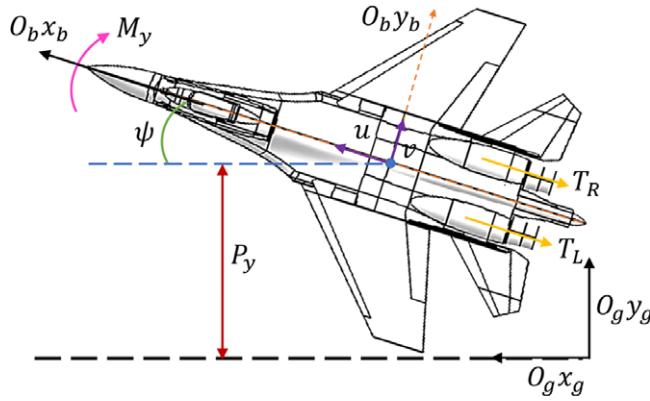


Figure 4. Force analysis of aircraft in transverse motion.

The lateral movement of the aircraft is affected by the aerodynamic forces and the engine thrust. In addition, the inertia forces and the loading model are equally significant. In this paper, the direction of the aircraft is controlled by the yawing moment. Figure 4 shows the force and moment of aircraft during the landing phase.

3.1 Aerodynamic force

Due to the vertical movement of the aircraft is ignored, the aerodynamic force consist of the drag F_D , side force F_C and yawing moment M_y . The forces and moments are described respectively in the air axis system ($O_a x_a y_a$) and the body axis system ($O_b x_b y_b$). The expressions of force and moment are as follows:

$$\begin{aligned}
 F_D &= \frac{1}{2} \rho_a V_a^2 S_w C_D \\
 F_C &= \frac{1}{2} \rho_a V_a^2 S_w C_C \\
 M_y &= \frac{1}{2} \rho_a V_a^2 S_w C_Y b
 \end{aligned}
 \tag{7}$$

where ρ_a is the air density and V_a is the aerodynamic velocity. S_w is the wing area, b is the wingspan, and c is the mean aerodynamic chord. C_D , C_C and C_Y are the aerodynamic coefficients. These coefficients are corresponding to the angle-of-attack α and the sideslip angle β . The aerodynamic angles can be calculated as:

$$\begin{aligned}
 \alpha &= \arctan \frac{w_a}{u_a} \\
 \beta &= \arctan \frac{v_a}{\sqrt{u_a^2 + w_a^2}}
 \end{aligned}
 \tag{8}$$

where u_a , v_a and w_a are the components of aerodynamic velocity in the body axis system ($O_b x_b y_b$). The force generated by the rudder is calculated in $O_a x_a y_a$

$$C_{\delta r} = \frac{1}{2} \rho_a V_a^2 S_r C_r \eta_r \delta_r n
 \tag{9}$$

The corresponding moment can be expressed in $O_b x_b y_b$:

$$Y_{\delta r} = -C_{\delta r} L_{\delta r}
 \tag{10}$$

where $S_r a$ is the rudder area and η_r is the efficiency of the rudder. δ_r is the control angle of deflection and C_r is the side force coefficient of the rudder. L_{δ_r} is the perpendicular distance between the force point on the rudder and the centre of gravity of the aircraft.

3.2 Dynamic equations of the aircraft

Before establishing the dynamic model, aerodynamic forces are converted to the body axis system. The direction of the force F_x is positive along $O_b x_b$ and F_y is positive along $O_b y_b$. The direction of the M_z is positive around $O_b x_b$. The expressions are as follows:

$$\begin{cases} F_x = -F_D \cos \beta - (F_C + C_{\delta_r}) \sin \beta \\ F_y = -F_D \sin \beta + (F_C + C_{\delta_r}) \cos \beta \\ M_z = M_y + Y_{\delta_r} \end{cases} \quad (11)$$

This study focuses on the lateral movement of carrier-based aircraft during landing process, which is considered as planar. The rolling, pitching and vertical dynamics are neglected. And the displacement along the $O_g x_g$ is also not account into the analysis of the landing safety boundary. Therefore, a3-DOF (five-dimensional) dynamic model is simplified to the following format:

$$\begin{cases} \dot{\psi} = r \\ \dot{P}_y = u \sin \psi + v \sin \psi \\ \dot{u} = rv + F_x/m \\ \dot{v} = -ru + F_y/m \\ \dot{r} = M_z/I_z \end{cases} \quad (12)$$

where ψ represent the yaw angle, P_y represent the lateral displacement which is defined as along the $O_g y_g$, m is the quality of the aircraft, I_z is the moment of inertia around the $O_b z_b$ axis, u is the longitudinal velocity, v is the lateral velocity and r is the angular velocity in yaw.

3.3 The particular H-J PDE for the viability

In order to obtain the safe boundary of the dynamic system, reachability theory is an effective method. According to Lygero’s description [14], a continuous time control system is considered:

$$\dot{x} = f(x, u) \quad (13)$$

where $x \in C \in R^n$, $u \in U \in R^m$, $f(\cdot, \cdot): R^n \times U \rightarrow R^n$ and C is the permissible state set determined by the system.

The viability is the set of states [20], which can remain in set C for time $t - T$ under permissible control, as shown in Fig. 5.

In this study, if the initial landing state is inside the unsafe set Q , no control law can be adopted to make the aircraft remain in the target set. The description of the viability by set is as follows:

$$Viab(t, C) = \{x \in R^n \mid \exists U, \forall \tau \in [t, T], x = \varphi(\tau, t, x, u(\cdot)) \in S\} \quad (14)$$

where $x = \varphi(\tau, t, x, u(\cdot))$ are the trajectories of the system and U is the permissible input.

The calculation of the controllable sets has been extensively studied in the last 20 years. A compelling method that involves a time-dependent H–J PDE is proposed. The method builds up a connection between viability and the SUPMIN optimal control problem.

Assume that the set C can be represented by a zero-level set of a continuous directional distance function: $l: R^n \rightarrow R$ by $C = \{x \in R^n \mid l(x) > 0\}$, the controllable set can be obtained by solving the following partial differential equations:

$$\frac{\partial V}{\partial t}(x, t) + \min \{0, H^*\} = 0 \quad (15)$$

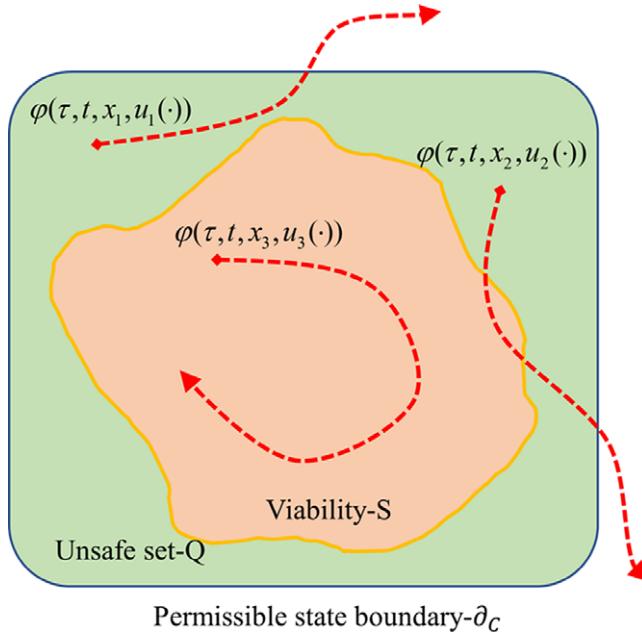


Figure 5. Controllable set diagram.

where $V(x, t) = l(x)$, $l(x)$ is the direction distance function of set C . The expression of the controllable set is as follows:

$$S = Viab(0, C) = \{x \in R^n \mid V(x, 0) > 0\} \tag{16}$$

In this paper, direction distance function $l(x)$ is defined as

$$l(x) = \min \{ \psi_{\max} - \psi, \psi - \psi_{\min}, D_{y\max} - D_y, D_y - D_{y\min} \} \\ \{ u_{\max} - u, u - u_{\min}, v_{\max} - v, v - v_{\min}, r_{\max} - r, r - r_{\min} \} \tag{17}$$

Hamiltonian is defined as:

$$H^* = \sup_{u \in U} p^T \cdot f(x, u) = p_1 \dot{\psi} + p_2 \dot{D}_y + p_3 \dot{u} + p_4 \dot{v} + p_5 \dot{r} \tag{18}$$

where $p_i (i = 1, 2, 3, 4, 5)$ is the spatial derivative of the state value for each dimension.

$$p = \nabla V(x) \tag{19}$$

Obviously, the analytic solution to the PDE of high dimensions is difficult to obtain. So, a numerical level set tools developed by Mitchell [12] are employed to obtain the viability of five-dimensional model. The tools are based on algorithms proposed by Osher and Fedkiw [21]. The optimal control corresponding to the maximum controllably set can be solved by equation (20). The value of μ^* maximise the Hamiltonian on the certain state:

$$\mu^* = \arg \sup_{u \in U} H^* \tag{20}$$

4.0 The safety boundary of arresting and rolling

4.1 Off-centre and yaw arrest matching envelope

After the aircraft touches down the carrier, the hook engages with the arresting cable and starts to slow down under the action of the arresting device, and the arresting trajectory should be along a part of

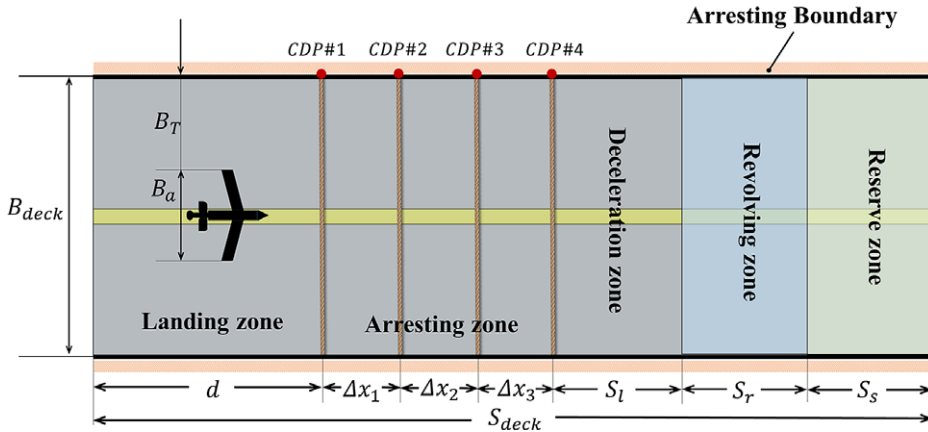


Figure 6. The compositions of angled deck.

the inclined deck on the carrier [22]. Since the direction of movement of the carrier-based aircraft is uncontrollable during the arresting, if the yaw angle or off-centre distance of the aircraft is too large before the arresting, the aircraft may impact the both sides of the blocking runway or parked aircraft on the deck. Figure 6 is the schematic diagram of the arresting and rolling process of carrier-based aircraft.

As shown in Fig. 6, it can be obtained:

$$\begin{cases} B_{deck} = B_a + 2B_T \\ S_{deck} = d + \Delta x_1 + \Delta x_2 + \Delta x_3 + S_l + S_r + S_s \end{cases} \quad (21)$$

where B_{deck} is the width of the landing runway, B_a is the wingspan of the aircraft, B_T is the distance between the aircraft wingtip and the safety boundary, S_{deck} is the length of runway, d is the length of landing zone, $\Delta x_1 + \Delta x_2 + \Delta x_3$ is the length of the arresting zone, S_l is the length of the deceleration zone, S_r is the length of the revolving zone and S_s is the length of the reserve zone.

In this section, it is assuming that $B_{deck} = 34m$, $B_a = 14m$ and $B_T = 10m$. At the end of the arresting, if the $B_T \leq 0$ when the aircraft is stop, the aircraft will rush out of the safe landing zone, and the accident may occur.

In this section, taking the lateral displacement of the carrier-based aircraft after being stopped by the arresting device as the research objective, the dynamic model of the aircraft arresting and rolling was established. Then taking the different landing speed v_h , yaw angle φ and off-centre distance D_y of the carrier aircraft as input parameters to perform batch simulation [23]. Monitor the value of B_T in real time during the process, and judge the critical operating conditions that exceed the safety cordon after the carrier-based aircraft stop. When B_T is greater than 0m, it means that the aircraft is stopped in the safe area, the input parameter constraint range as follows

$$\begin{cases} v_h = [40, 65], \quad \Delta v_h = 1m/s \\ D_y = [-12, 12] \quad \Delta D_y = 1m \\ \varphi = [-10, 10] \quad \Delta \varphi = 1^\circ \end{cases} \quad (22)$$

In the simulation results, the parameters satisfying B_T greater than 0m are extracted, and the three-dimensional representation diagram is drawn as shown in Fig. 7. In order to show the relationship between off-centre distance and yaw angle clearly, the 3D representation map is sliced at the landing speed of 55m/s, and the 2D projection map is obtained as shown in Fig. 8.

As shown in Fig. 7, the yaw angle and off-centre distance have a great impact on the arresting safety boundary of aircraft, while the landing speed has relatively little influence. As the landing speed increases, the range of the off-centre and yaw angle matching envelope gradually decreases. It means

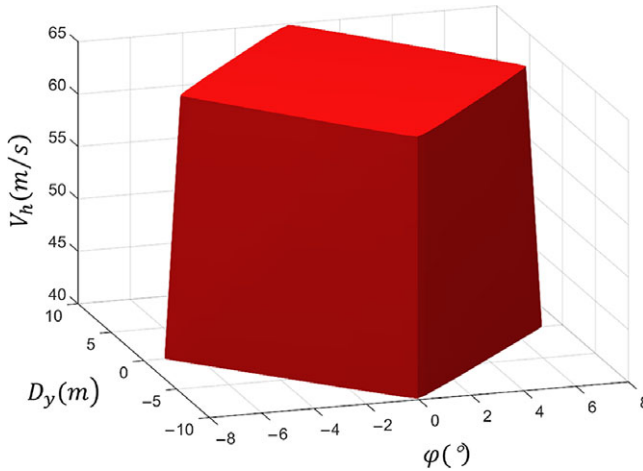


Figure 7. Arresting horizontal security boundaries.

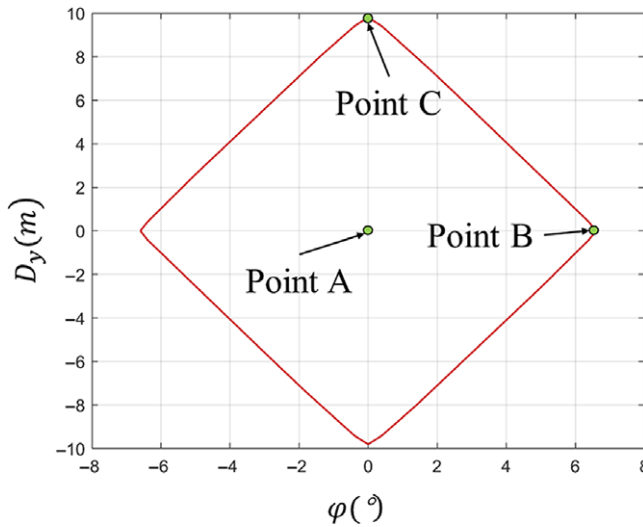


Figure 8. Projection of arresting horizontal security boundaries.

that the greater the landing speed of the carrier-based aircraft, the smaller the off-centre and yaw range that allow safe arresting during the interception process.

As shown in Fig. 8, the lateral dynamics safety boundary matching envelope of the aircraft arresting is centrally symmetrical. When the landing speed is 55m/s, the maximum safe yaw angle range is $(-6.2^\circ \sim +6.2^\circ)$, and the maximum safe eccentric distance range is $(-9.8m \sim +9.8m)$. It can be seen that if the carrier-based aircraft's yaw angle and off-centre distance are within the above range (Fig. 7), the aircraft can remain within the safe boundary after stopping and will not collide with the island or aircraft on both sides of the deck. This conclusion is similar to literature [11], which proves that the conclusion is accurate to some extent.

In order to verify the accuracy of the safety envelope obtained above, three representative key points are extracted from the obtained lateral dynamic safety boundary of arresting as parameters for the arresting dynamic simulation of carrier-based aircraft. The result as shown in Fig. 6, selected points are Point A($0^\circ, 0m$), Point B($6.2^\circ, 0m$) and Point C($0^\circ, 9.8m$). The selected three key points are taken as

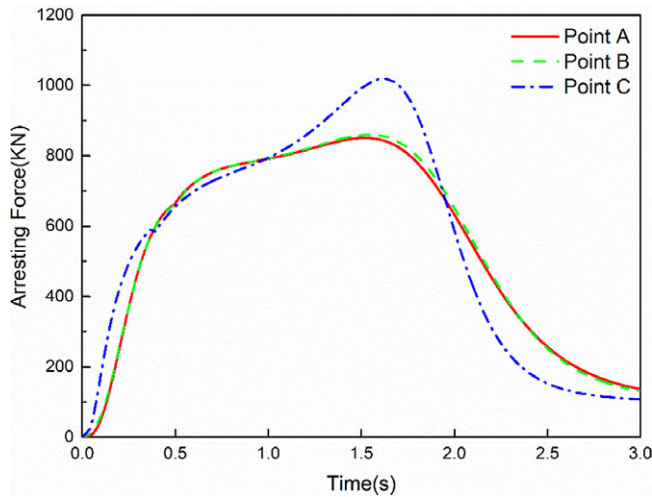


Figure 9. Curve of arresting force–time.

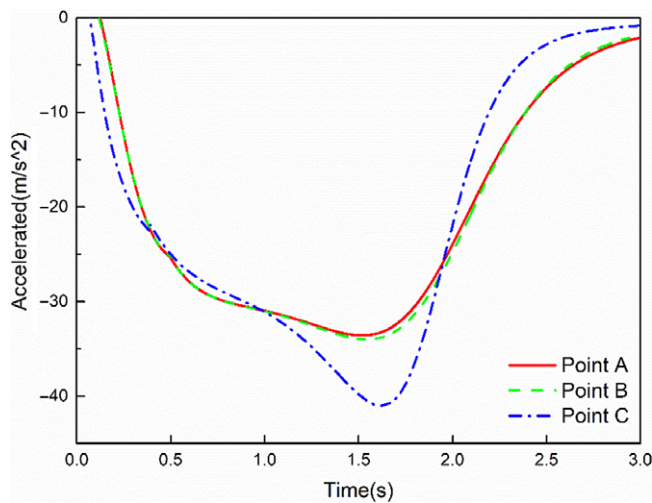


Figure 10. Curve of arresting acceleration–time.

parameters and brought into the carrier-based aircraft arresting dynamics model. The arresting force, acceleration, lateral displacement and velocity curve of the carrier-based aircraft during the arresting process are obtained, respectively, as shown in Figs. 9-12.

As shown in Fig. 9, at the time of 1.6s, the arresting force of aircraft reaches the maximum value. The maximum arresting force of Point B is 953.4KN, which is slightly greater than Point A(840.8KN). The maximum arresting force of Point C is 1018.6KN, which is greater than Point A and Point B. Due to the off-centre distance and the yaw angle of the aircraft are 0 under the condition Point A, it can be concluded that the existence of off-centre distance and yaw angle will increase the arresting force, and the arresting force is the smallest when the carrier-based aircraft is in symmetrical arresting.

Figure 10 shows the acceleration variation curve of carrier-based aircraft during arresting under the selected key point conditions. As shown in Fig. 10, the change trend of the acceleration is consistent with the change trend of the arresting force, but in the opposite direction. At the time of 1.6s, the arresting

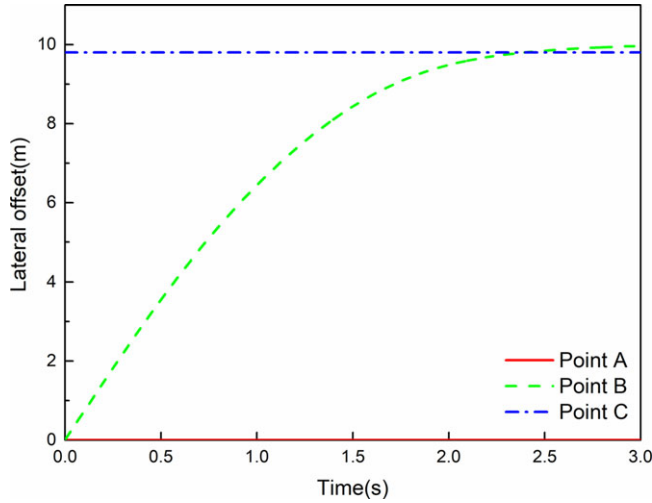


Figure 11. Curve of arresting lateral offset–time.

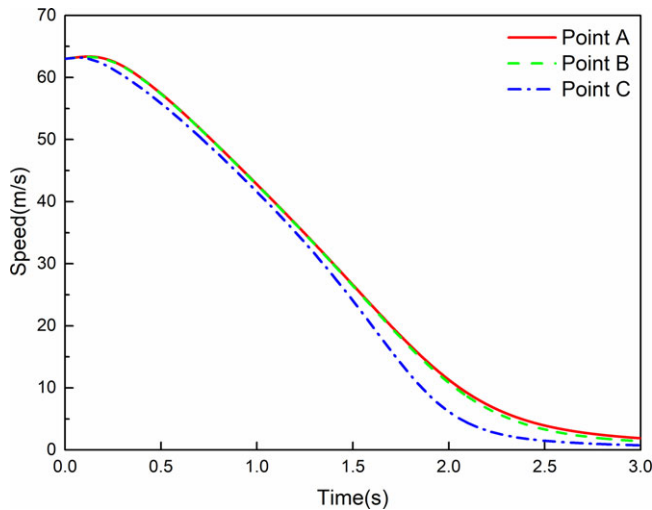


Figure 12. Curve of arresting speed–time.

acceleration of the three points reaches the maximum. The maximum acceleration of Point A is $-33m/s^2$, Point B is $-34m/s^2$ and Point C is $-41m/s^2$.

Figure 11 shows the curve of lateral displacement of carrier-based aircraft during arresting under the selected key point conditions. As shown in Fig. 11, the lateral displacement of carrier-based aircraft is equal to the off-centre distance in the conditions of Point A and Point C, the reason is that the yaw angle of aircraft is 0° . So the lateral displacement of Point A is 0m, and the lateral displacement of Point C is 9.8m. Under the condition of Point B, due to the existence of yaw angle, the lateral displacement of aircraft increases with time, and the maximum lateral displacement is 9.95 m at the end of arrest.

Figure 12 shows the curve of speed change of carrier-based aircraft during arresting under the selected key point conditions. It can be seen from the simulation results that the change trend of the deceleration curve of the aircraft at the three boundary points is similar. Under working condition Point C, due to the larger arresting force, its deceleration trend is slightly larger than Point A and Point B.

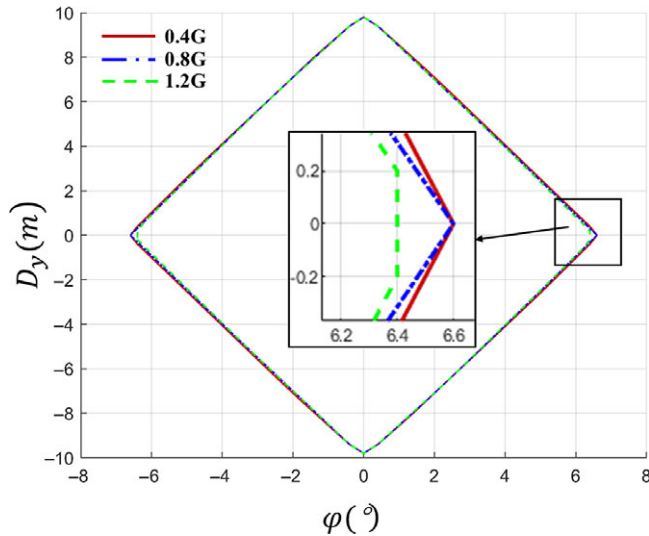


Figure 13. Influence of engine thrust on arresting lateral safety boundary.

Through the above analysis, it can be seen that three key points are selected in the above off-centre and yaw matching envelope for simulation. Under the key point conditions in the safety boundary, the carrier-based aircraft successfully realises the arresting and stopping, and the lateral displacement of the arresting process does not exceed the safety boundary, which proves that the obtained lateral safety boundary of arresting is reliable to some extent.

4.2 Influence of landing parameters on safe boundary of arresting

When the carrier-based aircraft is landing arresting, once the arresting hook is engaged with the arresting cable upon landing on the carrier, the pilot cannot control the arresting process. Typically, during this process, the pilot is required to control the engine thrust of the carrier-based aircraft to at least 40% of the aircraft weight [24] in order to be able to complete the re-flight operation after the arresting fails. According to the description in Reference [24], the weight of the aircraft is the key parameter affecting the arresting. Therefore, in order to study the influence of engine thrust and weight of the aircraft on the safety boundary of arresting taxiing, in this section, the original quality of carrier aircraft $M = 22680\text{kg}$, and $G = Mg = 226800\text{N}$. Different engine thrust and weight are selected for batch simulation. The engine thrust is taken as 40% G , 80% G and 120% G respectively, where G represents the weight of carrier-based aircraft. It is worth mentioning that the engine thrust depends on the weight of the carrier-based aircraft, when the weight of the aircraft is changed, the engine thrust also changes accordingly.

The simulation results are shown in Figs. 13 and 14.

As shown in Fig. 13, the change of engine thrust has an effect on the safety boundary of aircraft arresting, but the effect is small. The change of engine thrust will not change the maximum yaw angle of the safety boundary. The maximum range of off-centre distance decreases from 6.6 m to 6.4 m with the increase of the engine thrust from 40% G to 80% G , the area enclosed by the safety boundary increases by 1.1%, which means the safety boundary increases by 1.1%. When the engine thrust increases to 120% G , the safety boundary increases by 1.6%. According to the result in Fig. 14, the safe boundary has great influence under the change of aircraft weight. The reason is that with the change of aircraft weight, in order to ensure the well aerodynamic characteristics, engine thrust will change accordingly.

With the decrease of the weight of the carrier-based aircraft, the maximum yaw angle range of the safety boundary will not change, but the maximum safety off-centre distance decreases with the increase

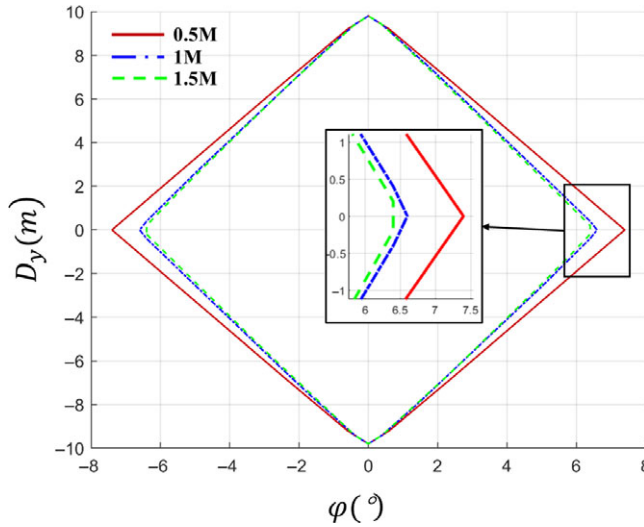


Figure 14. Influence of aircraft quality on arresting lateral safety boundary.

of the weight. When the quality of the aircraft is 0.5M, the maximum safety off-centre distance is 7.4m. The quality is M, the maximum safety off-centre distance is 6.6m and the safety boundary range increases by 9.2%. When the quality of the carrier-based aircraft is 1.5M, the maximum safety off-centre distance is 6.4m, and the safety boundary range increases by 10.7%.

4.3 Influence of landing parameters on the safety of arresting

In this section, a method for defining the safety evaluation index of the carrier-based aircraft arresting is proposed based on the lateral dynamic safety matching envelope in the above study, which lays the foundation for in-depth analysis of the influence of relevant parameters on the safety of the arresting and obtaining the parameter combination with the highest safety in the arresting.

4.4 Safety evaluation index of arresting

Through the above analysis, it can be seen that the lateral dynamic safety boundary of the carrier-based aircraft during the arresting is affected by the engine thrust and weight of the carrier-based aircraft. Considering the actual situation of the aircraft arresting process, it is defined that the smaller the lateral displacement of the carrier-based aircraft at the end of the arresting taxiing, the higher the arresting safety.

According to GJB67.4A3.1.19 [25], the various variables of carrier-based aircraft landing arrest are determined in a certain form of distribution, in which the aircraft longitudinal speed, yaw angle and off-centre distance are determined by Gaussian distribution function. Therefore, the value evaluation index of the aircraft during the arresting phase is defined by:

$$\begin{cases} Q_s = \frac{1}{\sqrt{B_T}} \cdot R_G(X_{sys}) \\ X_{sys} = \{v_h, D_y, \varphi\} \end{cases} \quad (23)$$

where Q_s is the value of each parameter combination, which is based on the three parameters of X_{sys} . $\frac{1}{\sqrt{B_T}}$ is the reference value for the current state and indicates that the smaller the lateral displacement of the carrier-based aircraft, the higher the value. The longitudinal velocity, yaw angle and off-centre

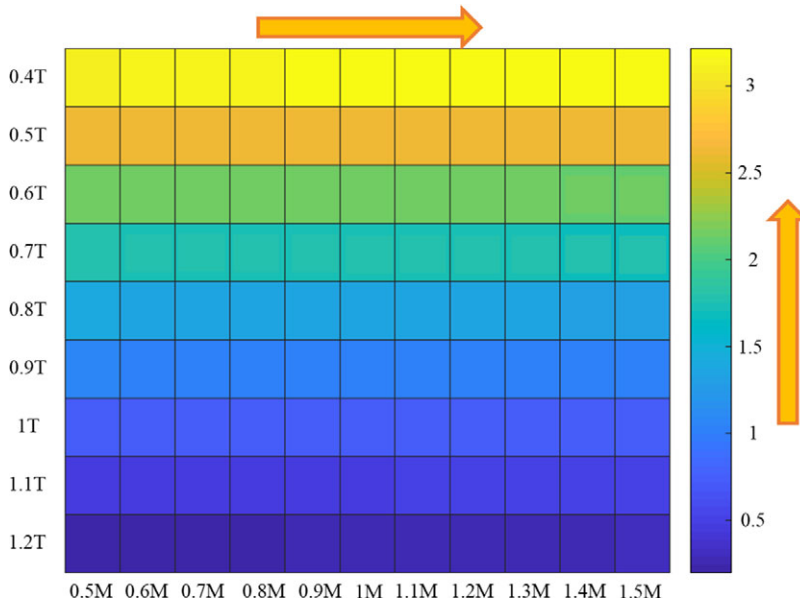


Figure 15. The variation trend of transverse safety of arresting under the influence of two-parameters.

distance of the aircraft are taken into Gauss function, and the cumulative product is taken as the value weight of the current state. The sum of values of all states within the safety boundary is used as the evaluation index of aircraft arresting safety.

4.5 Change rule of safety of arresting under the influence of two parameters

In the parameter range of formula (22), the simulation is carried out according to formula (23) of the value function, and the state value obtained by the simulation is processed to obtain the two-dimensional density map that reflects the safety value of arresting, as shown in Fig. 15.

As shown in Fig. 15, the safety of arresting decreases with the increase of engine thrust when the landing weight of the carrier-based aircraft is determined. And the safety of arresting decreases with the increase of engine thrust when the weight of the aircraft is determined.

It can be concluded that the engine thrust and landing quality should be minimised within the allowable range in order to ensure that the arresting and sliding process of shipborne aircraft does not exceed the lateral safety boundary. The smaller the thrust of the engine and the smaller the quality, the more conducive to improving the safety of the arresting.

5.0 Study on safe set of carrier-based aircraft landing process

Considering that the carrier aircraft should re-take-off in time after the arresting failure, set the longitudinal speed to 55m/s, engine thrust to 0.4Mg, weight of the aircraft to M, and the representation diagram about the lateral safety boundary of the carrier-based aircraft is depicted in Fig. 16. It means that the arresting taxiing of aircraft is safe when the yaw angle and off-centre distance are in the red envelope range.

However, the landing process of the carrier-based aircraft will always be affected by the wake and the sway of ship, even under the control of the landing guidance system, it is difficult to achieve fixed-point landing. Considering the solution calculation below ignore the influence of turbulence disturbance and carrier sway, the actual arresting safety boundary should be smaller than the red envelope in Fig. 16.

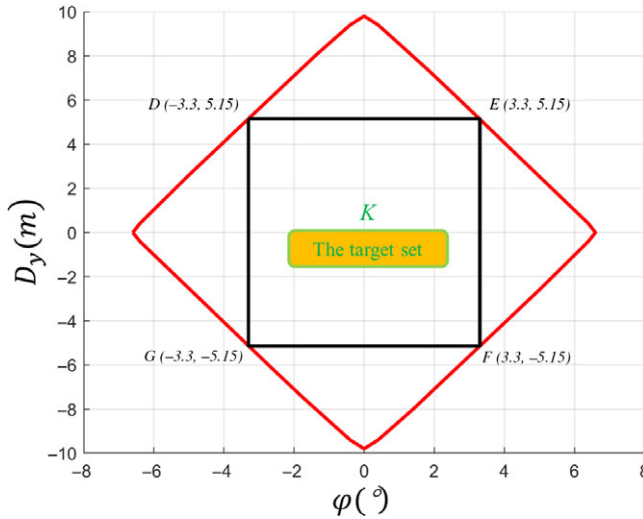


Figure 16. The lateral security boundary of arresting and the landing target area.

At the same time, in order to facilitate the calculation of the reachable set, this section selects the largest rectangle inscribed the red safety envelope, which is the arresting rectangle envelope in the Fig. 16 as the target set K of aircraft landing motion. The specific value are:

$$C^* = \{(\psi, P_y, u, v, r) \mid -3.1^\circ < \psi < 3.1^\circ, -5.15\text{m} < P_y < 5.15\text{m}, 40\text{m}/u < 65\text{m}/s, -30\text{m}/s < v < 30\text{m}/s, -30^\circ/s < r < 30^\circ/s\} \tag{24}$$

where ψ is the yaw angle, which corresponding the yaw angle φ of arresting, P_y is the lateral displacement, which corresponding the off-centre distance D_y of arresting.

Due to the high dimension and limited computing performance, the number of grids cannot be too large. The computing domain is divided into $25 \times 13 \times 23 \times 11 \times 11$ grids. In order to ensure the stability of numerical calculation, Hamiltonian is approximated numerically by global Lax–Friedrichs dissipation. Spatial derivative is calculated on a fifth-order weighted essentially no-oscillatory approximation. The partial differential equation is solved backward in time by the odeCFL3 integrator, which balances the work and the accuracy.

5.1 Results of landing lateral safe set

In order to visualise the safety boundary, high-dimensional results need to be sliced. Figure 17 shows the safety boundary of the other three dimensions when the initial lateral velocity and yaw angular velocity are 0. Axis of x, y, z represent yaw angle, lateral displacement and longitudinal velocity, respectively.

As shown in Fig. 17, under the optimal control input of rudder, the lateral safety boundary of carrier-based aircraft during landing is centrally symmetric, and its lateral displacement and yaw angle range decreases with the increase of longitudinal speed. When the longitudinal speed is 40 m/s, the maximum safe yaw angle is $\pm 1.13^\circ$, and the safe lateral displacement is ± 4.58 m. When the longitudinal speed is 64 m/s, the maximum safe yaw angle is $\pm 0.77^\circ$, and the lateral displacement distance is ± 4.58 m. When the longitudinal speed is 55m/s, the two-dimensional safety boundary is obtained by slicing Fig. 17, as shown in Fig. 18. The maximum safe yaw angle is $\pm 0.9^\circ$, and the safe lateral displacement distance is ± 4.6 m. When the carrier-based aircraft landing at a longitudinal speed of 55m/s, keep the yaw angle in the range of $(-0.9^\circ \sim + 0.9^\circ)$, and the lateral displacement in the range of $(-4.6\text{m} \sim + 4.6\text{m})$, the carrier-based aircraft can successfully reach the target set under the optimal control of the rudder, and complete the arresting safely.

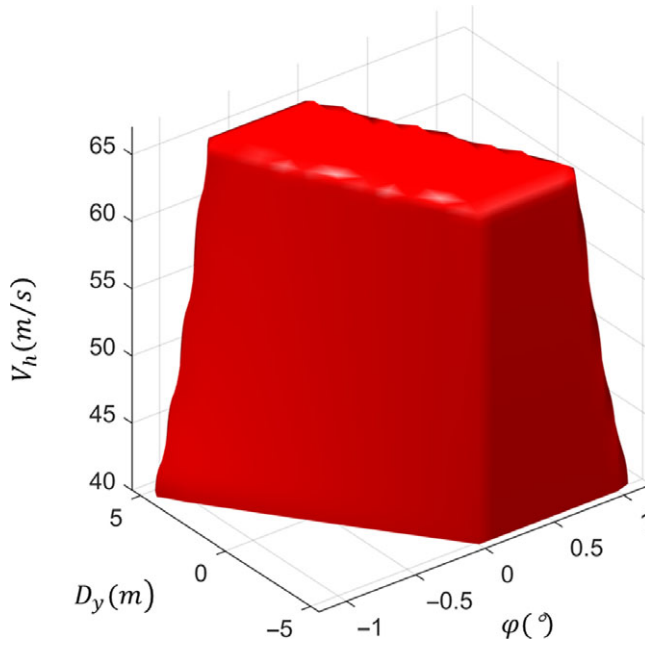


Figure 17. Lateral safety boundary during landing descent.

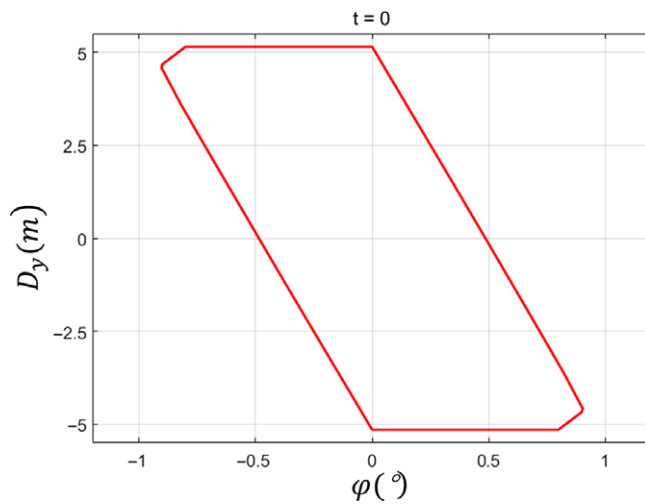


Figure 18. Safety boundary section when longitudinal speed is 55m/s.

5.2 Analysis of the influence of parameters on safe set

In this section, the engine thrust T and quality of the carrier-based aircraft M in the landing phase are selected as the parameters to analyse the influence of its change on the lateral safe set.

5.2.1 The influence of engine thrust

Figure 19 shows the calculation results of the safe set under the original engine thrust T and 140% T . Figure 20 is the two-dimensional envelope curve under the longitudinal speed is 55 m/s.

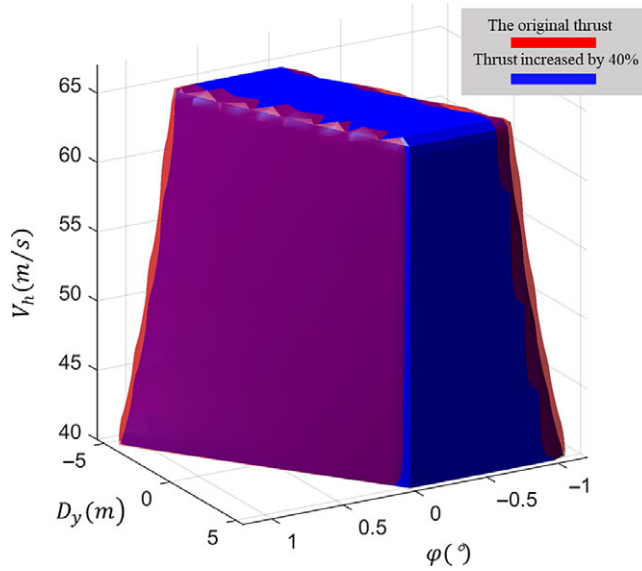


Figure 19. Lateral safety boundary of landing glide process under the influence of different engine thrust.

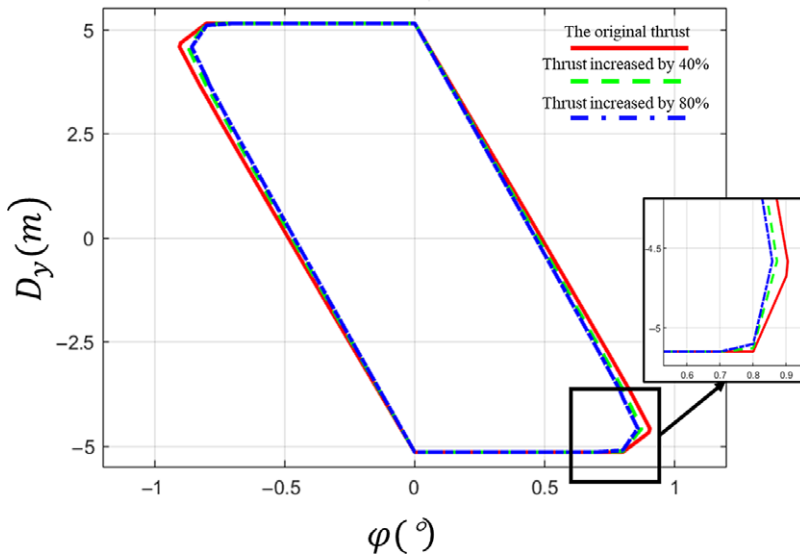


Figure 20. Safety boundary section when longitudinal speed is 55m/s.

It can be concluded that when the longitudinal speed is 55 m/s, the increase of engine thrust by 40% reduces the maximum safe yaw angle of aircraft from 0.9° to 0.87° , and reduces the safe boundary range by 4.2%. When the engine thrust increases to 80%, the maximum safety yaw angle of the aircraft decreases from 0.87° to 0.86° , and the safety boundary range decreases by 5.5%. It can be seen that the carrier-based aircraft cannot blindly increase the engine thrust during the landing glide process. Increasing the engine thrust will reduce the lateral safety boundary, thereby reducing the safety of the landing arrest.

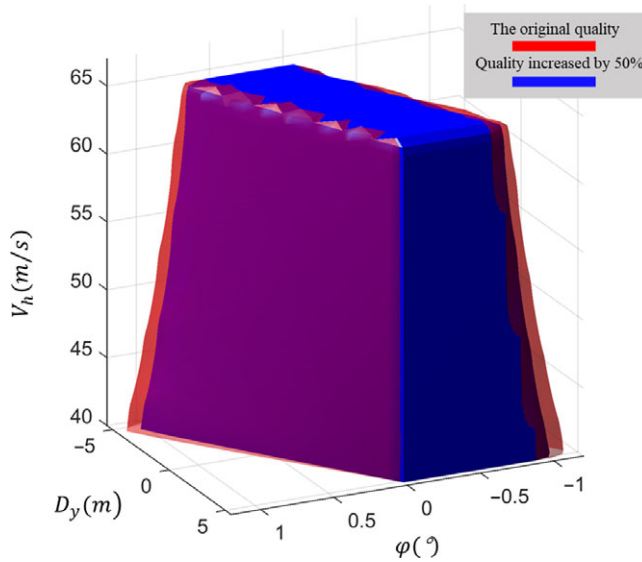


Figure 21. Lateral safety boundary of landing glide process under the influence of different aircraft quality.

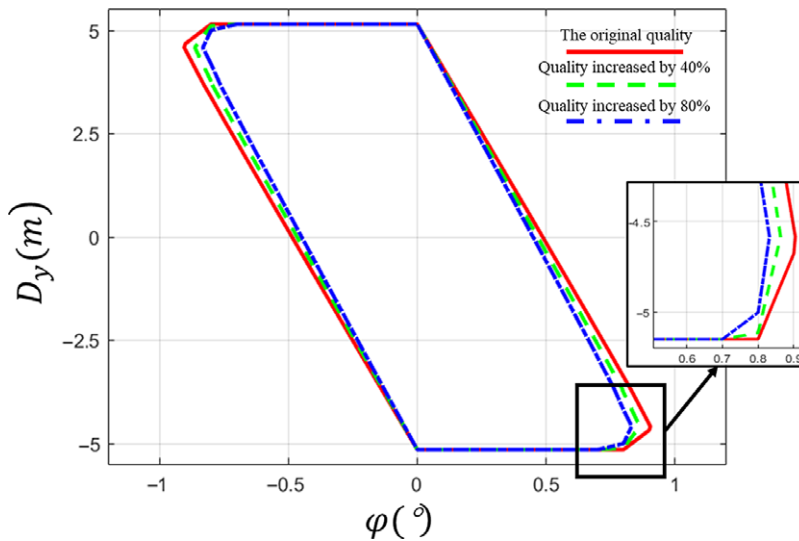


Figure 22. Safety boundary section when longitudinal speed is 55m/s.

5.2.2 Influence of aircraft quality

Figures 21 and 22 show the safe set of the original quality of aircraft, quality increase of 40% and quality increase of 80%, respectively.

It should be pointed out that when the quality of the carrier-based aircraft is changed, engine thrust should be guaranteed to be 40% of carrier aircraft quality. With the increase of the landing quality, the engine thrust will also increase accordingly.

As shown in the Figs. 21 and 22, the maximum safety yaw angle decreases from 0.9° to 0.86° with the quality of the carrier-based aircraft increases, and the lateral safety boundary range decreases

by 2.8%. When the quality of the carrier-based aircraft increases by 80%, the maximum safety yaw angle decreases from 0.9° to 0.83° , and the lateral safety boundary range decreases by 3.7%, showing a decreasing trend.

6.0 Conclusion

The research in this study aims at the safety problems caused by the limited landing space of the carrier deck in the process of aircraft landing arresting. By establishing the dynamic model of arresting taxiing of carrier-based aircraft, the lateral safety boundary of deck arresting is obtained based on batch simulation. On this basis, the lateral safe flight area during the landing glide is inversely deduced based on the specific Hamilton-Jacobi partial differential equation in the reachable set theory. Subsequently, the influence of key parameters on set set is analysed, and some important conclusions are summarised as follows:

1. The dynamic model of the arresting of carrier-based aircraft is established. With the help of batch simulation method, the lateral dynamic safety envelope of aircraft in arresting and sliding is defined, and the influence of landing parameters on safety envelope is analysed. The results show that with the increase of engine thrust and landing quality, the lateral safety boundary of arresting on the deck decreases.
2. The boundary points on the safety boundary on the deck are extracted, and the dynamic characteristics of the arresting process of the aircraft at the boundary points of the safety boundary are analysed. The results show that the obtained state quantities in the safety boundary can realise the safe arrest of the carrier aircraft.
3. Based on the obtained lateral dynamic safety envelope of arresting taxiing, the target set of the landing stage of carrier-based aircraft is reasonably defined, and the lateral dynamic safety boundary of the landing stage of aircraft is obtained by the method of reachable set. The influence of key parameters on aircraft safety envelope is studied. The results show that based on the optimal control rate of rudder, the lateral safety envelope of carrier-based aircraft in the landing guidance phase decreases with the increase of engine thrust and landing quality.

In this study, a dynamic safety analysis method for the safety of landing arrest is proposed. The research results are of great significance for the improvement of the landing and arresting safety of aircraft, which can provide theoretical guidance and technical reserves for subsequent related research.

Funding. This study was funded by the National Defense Excellence Youth Science Fun of China (2018-JCJQ-ZQ-053), the China Postdoctoral Science Foundation (2019M651827), Jiangsu Planned Projects for Postdoctoral Research Funds (2018K042B).

References

- [1] Zeng, T. Research on the influence of atmospheric disturbances on the carrier-based aircraft' distribution of touchdown point[D]. Xiamen University, 2018.
- [2] Xie, P., Peng, Y., WEI, X. and NIE, H. Dynamic analysis of off-center arrest for carrier-based aircraft considering kink-wave[J]. *J. Beijing Univ. Aeronaut. Astronaut.*, 2020, **46**, (08), pp 1582–1591.
- [3] Yang, Y. *Review of the carrier approach criteria[M]*, National Defense Industry Press, 2006, Beijing, pp 59–63(in Chinese).
- [4] The Chief Committee of Aircraft Design Manual. *Air-craft designmanual: Take-off and landing system design*, Aviation Industry Press, 2002, Beijing, pp 271–280 (in Chinese).
- [5] Rudowsky, T., Hynes, M., Luter, M., Niewoehner, R. and Senn, P. Review of the Carrier Approach Criteria for Carrier-Based Aircraft–Phase I; Final Report, 2002/71.
- [6] MIL-A-8863C. Airplane Strength and Rigidity, ground loads for carrier-based aircraft[S]. Naval Air Systems Command, 1993.
- [7] Lawrence, J.T. Milestones and developments in US naval carrier aviation-part II: AIAA-2005-6120. In Reston: AIAA. Proceedings of the AIAA Atmospheric Flight Mechanics Conference and Exhibit, San Francisco, CA, USA, 15–18 August 2005.

- [8] Hsin, C. Arrested Landing Studies for STOL aircraft, A73-17627 (AH); American Institute of Aeronautics and Astronautics, Annual Meeting and Technical Display: Washington, DC, USA, 1973.
- [9] Zhang, Z.K., Nie, H. and Yu, H. Dynamics Analysis for Aircraft Arresting with Yawing and Off-center, *Ad Aeroiaut. Sci. En.*, 2010, **1**, pp 327–332.
- [10] Zhang, S.S. and Jin, D.P Nonlinear optimal control of aircraft arresting process. *Acta Aeronaut. Astronaut. Sinica.*, 2009, **30**, pp 849–854
- [11] Peng, Y., Xie, P., Wei, X. and Nie, H. Dynamic analysis and security characteristics of carrier-based aircraft arresting in yaw condition. *Applied Sciences*, 2020, **10**(4).
- [12] Mitchell, I.M. A toolbox of level set methods. UBC Department of Computer Science Technical Report TR-2007-11 2007.
- [13] Mitchell, I.M., Bayen, A.M. and Tomlin, C.J. A time-dependent Hamilton-Jacobi formulation of reachable sets for continuous dynamic games, *IEEE Trans. Automat. Control.*, 2005, **50**, (7), pp 947–957.
- [14] Lygeros, J. On reachability and minimum cost optimal control. *Automatica*, 2004, **40**, (6), pp 917–927.
- [15] Allen, R., Kwatny, H. and Bajpai, G., “Safe Set Protection and Restoration for Unimpaired and Impaired Aircraft,” (2012).
- [16] Oishi, M., Mitchell, I., Tomlin, C. and Saint-Pierre, P. Computing Viable Sets and Reachable Sets to Design Feedback Linearizing Control Laws Under Saturation. IEEE Conference on Decision and Control, 2008
- [17] Wang, X.F., Li, J.M., Kong, X.W., Dong, X.M. and Zhang, B. Towards docking safety analysis for unmanned aerial vehicle probe-drogue autonomous aerial refueling based on docking success-probability and docking reachability. *Proc. Inst. Mech. Eng. J. Aerosp. Eng.*, 496 2018, **233**, (11), pp 3893–3905.
- [18] Meng, X. The Research on Some Key Problems in General Arrangement Design of Flight Deck[D]. Harbin Engineering University, 2011.
- [19] Liu, G. and Nie, H. Dynamics analysis for aircraft arresting based on absorbing aircraft kinetic energy[J]. *China Mech. Eng.*, 2009, **20**, (4), pp 450–454 (in Chinese).
- [20] Liang T, Yin Q, Fang W, et al. The maximum taxiing safe set of the wheel-skid aircraft under optimal control of rudder[J]. *Proc. Inst. Mech. Eng. Part G J. Aerosp. Eng.*, 2021: 095441002199538
- [21] Osher, S. and Fedkiw, R. *Level Set Methods and Dynamic Implicit Surfaces*, Springer-Verlag, 2002.
- [22] Huafeng, G.A.O. Research on the Rigid-flexible Coupling Dynamics of Carrier-based Aircraft Arrested Deck-landing Under[D]. South China University of Technology, 2018.
- [23] Zhang, Z., Peng, Y., Wei, X., Nie, H., Chen, H. and Li, L. Research on parameter matching characteristics of pneumatic launch systems based on co-simulation. *Aeronaut. J.*, 2021, 1–25. doi: [10.1017/aer.2021.70](https://doi.org/10.1017/aer.2021.70)
- [24] Zhang, X. *Dynamic Analysis And Simulation Of Carrier Aircraft Arrested Deck-Landing*, Northwestern Polytechnical University, 2007.
- [25] General Armament Department of the Chinese People’s Liberation Army. Specification for structural strength of military aircraft - Part 4: The ground load: GJB 67.4A’2008. Beijing: General Armament Department of the People’s Liberation Army, 2008.